JOURNAL OF THERMOPHYSICS AND HEAT TRANSFER
Vol. 23, No. 2, April–June 2009

Fire II Flight Experiment Analysis by Means of a Collisional-Radiative Model

Marco Panesi*
von Kármán Institute for Fluid Dynamics, 1640 Rhode-St.-Genèse Belgium
Thierry Magin†
Stanford University, Stanford, California 94305
Anne Bourdon‡
Ecole Centrale Paris, 92295 Châtenay-Malabry Cedex, France
Arnaud Bultel§
Université de Rouen, 76800 Saint Etienne du Rouvray Cedex, France
and
O. Chazot¶
von Kármán Institute for Fluid Dynamics, 1640 Rhode-St.-Genèse Belgium

DOI: 10.2514/1.39034

We study the behavior of the excited electronic states of atoms in the relaxation zone of one-dimensional airflows obtained in shock-tube facilities. A collisional-radiative model is developed, accounting for thermal nonequilibrium between the translational energy mode of the gas and the vibrational energy mode of individual molecules. The electronic states of atoms are treated as separate species, allowing for non-Boltzmann distributions of their populations. Relaxation of the free-electron energy is also accounted for by using a separate conservation equation. We apply the model to three trajectory points of the Fire II flight experiment. In the rapidly ionizing regime behind strong shock waves, the electronic energy level populations depart from Boltzmann distributions because the high-lying bound electronic states are depleted. To quantify the extent of this nonequilibrium effect, we compare the results obtained by means of the collisional-radiative model with those based on Boltzmann distributions. For the earliest trajectory point, we show that the quasi-steady-state assumption is only valid for the high-lying excited states and cannot be extended to the metastable states.

I. Introduction

DURING a hypersonic entry into the Earth's atmosphere, a massive amount of the freestream kinetic energy is converted into translational energy of the gas across a strong shock wave. Depending on the intensity of the shock, different physicochemical processes may take place, such as excitation of the internal energy modes, dissociation of the molecules, and ionization of the atoms and molecules. These nonequilibrium phenomena are strongly coupled to each other. At high reentry speeds, a significant portion of the heating experienced by the spacecraft can be due to radiation and is highly influenced by the shape of the internal energy distribution function. Concentration of the gas species and distribution of their internal energy level populations can be estimated by means of either multitemperature models [1–3] or collisional-radiative (CR) models [4–6].

In the case of multitemperature models [2], the physicochemical properties of the airflow are obtained through the shock layer by assuming that, for all species, the population of each internal (rotational, vibrational, or electronic) energy mode follows a Boltzmann distribution at a specific temperature (rotational T_r, vibrational T_v, or electronic temperature T_e). To calculate these temperatures and the energy exchanged between all the energy modes (i.e., translational, rotational, vibrational, and electronic), conservation equations for the internal energy modes in thermal nonequilibrium are added to the classical set of conservation equations for mass, momentum, and total energy. For the chemical kinetics model, macroscopic rate coefficients are assumed to depend on an empirical temperature that is a function of the different temperatures in the flow. It is important to mention that multitemperature models are easy to implement in multidimensional flow codes and have been used extensively in the literature so far [2,7–11].

Park (for example, in [2,12]) has extensively worked on multitemperature models for air and has also shown that the internal energy level populations may depart from Boltzmann distributions in expanding and compressing flows. Therefore, the use of multitemperature models, even if very efficient from a computational point of view, can only be justified when the departure from the Boltzmann population is small (i.e., for low velocity and high pressure reentry conditions).

Collisional-radiative models take into account all relevant collisional and radiative mechanisms between the internal energy levels of the different species present in the flow. They constitute a valid alternative to the multitemperature models because they exhibit a larger spectrum of applicability. By increasing the order of complexity and computational time, three kinds of CR models can be distinguished for air: *electronic* [13–16], *vibrational* [12,17], and

Presented as Paper 4023 at the 38th AIAA Plasmadynamics and Lasers Conference, Miami, FL, 25–28 June 2007; received 11 June 2008; revision received 6 November 2008; accepted for publication 14 November 2008.

*Ph.D. Candidate, Department of Aeronautics and Aerospace, 72 Chaussée de Waterloo; panesi@vki.ac.be. Member AIAA.

†Postdoctoral Fellow, Center for Turbulence Research, 488 Escondido Mall; magin@stanford.edu.

‡Research Scientist, Laboratoire Energétique Moléculaire Macroscopique et Combustion, Unité Propre de Recherche 288, Centre National de la Recherche Scientifique; anne.bourdon@em2c.ecp.fr.

§Assistant Professor, Complexe de Recherche Interprofessionnel en Aérothermochimie, Centre National de la Recherche Scientifique, Unite Mixte de Recherche 6614, Centre National de la Recherche Scientifique; arnaud.bultel@coria.fr.

¶Associate Professor, Department of Aeronautics and Aerospace, 72 Chaussée de Waterloo; chazot@vki.ac.be.

rovibrational state-to-state models. In electronic state-to-state models, transitions between the electronic states are considered and the rovibrational levels of the molecules are populated according to Boltzmann distributions at temperatures T_v and T_r. In vibrational state-to-state models, transitions between the vibrational states of the molecules are also considered and only a rotational temperature is defined. For both types of models, intensive requirements in terms of computational power do not allow for efficient implementation in multidimensional codes; most calculations are thus performed by means of 0-D and 1-D flow solvers. Finally, in rovibrational state-to-state models, no internal temperature is required. Note that rovibrational models have not been proposed so far, due to the computational power limitations and lack of knowledge of the reaction rates.

When using CR models, we distinguish several ways to deal with time integration and coupling with flow solvers. The most widely used approach for time integration is the quasi-steady-state (QSS) approximation [13,18]. This method is based on the simplifying assumption that the characteristic time of processes involving excited states is extremely fast compared with that of the flow; therefore, concentrations of the species on excited states adjust almost instantaneously to the flow changes. The QSS assumption can be used either for all excited levels or only for a limited number of them (e.g., high-lying electronic levels). Various QSS CR models have been developed for air [15–17] and used in 0-D. For example, the electronic state-to-state models given in [15–17] and the vibrational state-to-state model in [17] have been developed to study nonequilibrium effects in recombining plasmas at atmospheric pressure characterized by a free-electron temperature larger than the heavy-particle temperature.

QSS CR models can be loosely coupled to flow codes [2,13]; the profiles of the thermodynamic variables (pressure and temperatures) and species mass fractions are derived based on a flow calculation, then the populations of excited states are obtained at each desired location in the flow by means of a QSS CR model [2]. Johnston [13] has used this approach (QSS electronic state-to-state CR model [19]) to study the influence of the nonequilibrium distribution of the electronic energy levels of atoms and molecules of air after a strong shock. He has shown that nonequilibrium populations strongly affect the radiative heat fluxes.

The second approach for time integration is the so-called time-dependent CR model, in which balance equations are solved simultaneously for all species in ground and excited states, without any constraint on the relaxation times of the excited levels. Recently, a time-dependent electronic state-to-state CR model for air has been developed and used in 0-D in [14]. Different typical reentry flow conditions have been studied, and significant differences have been observed between the species concentrations calculated with the CR model and the widely used multitemperature kinetic mechanisms of Dunn and Kang [20], Park [21], and Gupta et al. [22].

Time-dependent CR models can be either loosely or directly coupled to flow codes. The loosely coupled, or Lagrangian approach, is particularly well adapted when the concentrations of excited states are much lower than those of the ground state. In this method, the profiles of the thermodynamic variables (pressure and temperatures) and the mass fractions of species are also derived based on a flow computation. In a second step, the excited species mass fractions are then obtained by following accurately in time a cell of fluid. For example, this method has been used for entries into the atmosphere of Titan [23]; for low pressure conditions, significant deviations of the excited-electronic-state populations of nitrogen molecules from QSS predictions have been observed in the near-shock region.

In the directly coupled approach, state-to-state equations are solved simultaneously with classical conservation equations of the flow; this approach is the most general one. In [5,24], vibrational nonequilibrium has been studied in supersonic air nozzle flows, and Park [12] has shown that the populations of upper vibrational levels deviate from a Boltzmann equilibrium and are strongly affected by the air chemistry (in particular, by the Zel'dovich reaction between molecular nitrogen and atomic oxygen).

In this work, we propose to study Fire II [25], a reentry flight experiment carried out in the 1960s. One of the primary objectives of the Fire project was to estimate the heating that a capsule experiences at high-speed conditions ($\geq$ 10 km/s). The focus of this project was the estimation of the radiative component of the heat flux by directly measuring the incident radiation using onboard radiometers. Moreover, the data collected from the experiment can be used for the validation of the flow solver and physical models [13,26,27].

In the analysis that follows, we focus our attention on three different points in the trajectory: 1634, 1636, and 1643 s (elapsed time from the launch). The first two points chosen belong to the earlier part of the trajectory, in which the flow exhibits strong nonequilibrium effects, whereas for the last point under consideration, the gas is close to equilibrium conditions.

The investigation is carried out by means of a hybrid model that combines the use of an electronic state-to-state CR model for the electronic levels of the atoms and describes the thermal nonequilibrium effects of the other energy modes by means of a multitemperature model. The choice of the atoms is justified by the fact that for the high temperatures reached at high speeds ($\geq$ 10 km/s), the contribution to the radiative component of the heat flux is dominated by atomic lines and continuum radiation [13,28,29], and the molecules are almost completely dissociated in this temperature range.

The rates of the electronic-specific reactions are based on the data of the electronic state-to-state CR model recently developed by Bultel et al. [14]. A complementary set of reaction rates is taken from Park et al. [30]. In this work, the time-dependent CR model is directly coupled with a one-dimensional flow solver to simulate shock-tube experiments. Then conservation equations of mass, momentum, global energy, vibrational energy, and free-electron energy are solved simultaneously.

The large number of elementary processes considered in the model will allow for a better understanding of the kinetic mechanisms for air plasmas, enabling us to better reproduce the gas kinetics in the shock layer and also describe the electronic energy level populations used to estimate radiative heat fluxes. Furthermore, as the state-to-state CR model is directly coupled to the flow solver, a thorough analysis of the validity of the QSS assumption is also carried out.

The physical model is presented in Sec. II, with a description of the CR part and the multitemperature part of the model. Section III is devoted to simulations of shock-tube flows representative of the Fire II flight experiment. A comparison with results from literature [13,31] is performed. Then validity of the QSS assumption is discussed, comparing three different formulations with the fully coupled approach described in Sec. II.

II. Physicochemical Modeling

The air mixture used in this work comprises 95 species, including the electronic energy levels of atomic nitrogen and oxygen. The vibrational energy level populations of the N_2, O_2, and NO molecules are assumed to follow Boltzmann distributions at the vibrational temperatures T_{vN_2}, T_{vO_2}, and T_{vNO}, respectively; the vibrational populations of the other molecules are associated with the vibration of the N_2 molecule. The rotational energy level populations are assumed to follow Boltzmann distributions at the translational temperature T of the gas. The CR model yields the electronic state populations of the N and O atoms. Thus, their electronic temperature does not need to be specified. The electronic energy populations of the other species are assumed to follow Boltzmann distributions at the translational temperature T_e of the free electrons.

A. Air Mixture

In this study, air is considered as a mixture of nitrogen and oxygen and their products are composed of 1) neutral species N_2, O_2, NO, N(1–46), and O(1–40) and 2) charged species N_2^+, O_2^+, NO^+, N^+, O^+, and e^-.

Forty-six electronic energy levels for N and 40 levels for O are accounted for in Table 1. They allow us to accurately calculate

Table 1 Index, energy, degeneracy, and secondary quantum number for the N and O electronic energy states considered

k for N(k)	E_k, eV	g_k	l_k	k for O(k)	E_k, eV	g_k	l_k
1	0.000	4	1	1	0.000	9	1
2	2.384	10	1	2	1.970	5	1
3	3.576	6	1	3	4.190	1	1
4	10.332	12	0	4	9.146	5	0
5	10.687	6	0	5	9.521	3	0
6	10.927	12	1	6	10.740	15	1
7	11.603	2	1	7	10.990	9	1
8	11.759	20	1	8	11.838	5	0
9	11.842	12	1	9	11.930	3	0
10	11.996	4	1	10	12.090	25	2
11	12.006	10	1	11	12.100	15	2
12	12.125	6	1	12	12.300	15	1
13	12.357	10	0	13	12.370	9	1
14	12.856	12	0	14	12.550	15	0
15	12.919	6	0	15	12.670	5	0
16	12.972	6	2	16	12.710	3	0
17	12.984	28	2	17	12.740	5	0
18	13.000	26	2	18	12.760	25	2
19	13.020	20	2	19	12.770	15	2
20	13.035	10	2	20	12.780	56	3
21	13.202	2	1	21	12.860	15	1
22	13.245	20	1	22	12.890	9	1
23	13.268	12	1	23	13.030	5	0
24	13.294	10	1	24	13.050	3	0
25	13.322	4	1	25	13.080	40	2
26	13.343	6	1	26	13.087	56	3
27	13.624	12	0	27	13.130	15	1
28	13.648	6	0	28	13.140	9	1
29	13.679	90	2	29	13.220	5	0
30	13.693	126	3	30	13.230	3	0
31	13.717	24	1	31	13.250	168	2
32	13.770	2	1	32	13.330	5	0
33	13.792	38	1	33	13.340	3	0
34	13.824	4	1	34	13.353	96	2
35	13.872	10	1	35	13.412	8	0
36	13.925	6	1	36	13.418	40	2
37	13.969	18	0	37	13.459	8	0
38	13.988	60	2	38	13.464	40	2
39	13.999	126	3	39	13.493	3	0
40	14.054	32	1	40	13.496	40	2
41	14.149	18	0	——	——	——	——
42	14.160	90	2	——	——	——	——
43	14.164	126	3	——	——	——	——
44	14.202	20	1	——	——	——	——
45	14.260	108	0	——	——	——	——
46	14.316	18	0	——	——	——	——

1) ionization of the N and O atoms by electron impact and 2) the net population of the metastable states N(2) = N($^2D^0$), N(3) = N($^2P^0$), O(2) = O(^1D), and O(3) = O(^1S) resulting from electron-induced processes. Coupling of the atom electronic energy levels through the different elementary processes considered in the following section allows for explicit determination of their excitation and the radiative signature of the plasma without using any a priori assumption on their populations.

Although the O_2^- and O^- species can also be formed, their contribution to chemistry can be considered to be negligible, as a result of the high temperature level reached behind the shock wave and the high rate coefficient for detachment processes that follow.

B. Collisional-Radiative Model

1. *Atomic Elementary Processes*

The inelastic collisions between the mixture species lead to chemical changes. The N and O atoms are efficiently excited and ionized by electron-impact reactions; due to their weak mass, free electrons very easily change occupation of the attached electrons of atoms. Several models exist for the related cross sections and rate coefficients. For excitation and ionization of the first three states of N and O, we have used the rate coefficients reported by Bultel et al. [14]. Their collisional-radiative model for air has been previously used for weaker shock conditions (speeds of 5–6 km/s).

The cross sections proposed by Drawin [32,33] proved to be efficient in similar conditions and are thus adopted here for excitation and ionization of the higher states. We have expressed the rate coefficients under an analytical form derived from integration of these cross sections over a Boltzmann distribution at the electron T_e. For an electronic transition from the i to j level, where $j > i$, the rate coefficient $k_{i\to j}$ is a function of the secondary quantum number l of each level involved

For an optically allowed transition ($l_i \neq l_j$),

$$k_{i\to j} = 4\pi v_e a_0^2 \alpha \left(\frac{E_H}{k_B T_e}\right)^2 I_1(a) \tag{1}$$

where quantity $v_e = [8RT_e/(\pi M_e)]^{1/2}$ is the electron thermal speed, R is the universal gas constant, M_e is the electron molar mass, $a_0 = 0.529 \times 10^{-10}$ m is the first Bohr radius, $E_H = 13.6$ eV is the ionization energy of the hydrogen atom, $\alpha = 0.05$, and

$$I_1(a) = 0.63255 a^{-1.6454} \exp(-a)$$

with the reduced energy

$$a = \frac{E_j - E_i}{k_B T_e}$$

For an optically forbidden transition ($l_i = l_j$),

$$k_{i\to j} = 4\pi v_e a_0^2 \alpha \left(\frac{E_j - E_i}{k_B T_e}\right)^2 I_2(a)$$

with the same notations and where quantity

$$I_2(a) = 0.23933 a^{-1.4933} \exp(-a)$$

The reverse processes are based on the microreversibility principle, and the reverse rate is calculated from the equilibrium constant

$$K_{\text{eq}}(T_e) = \frac{g_j}{g_i} \exp(-a)$$

For ionization of an atom under electron impact, Eq. (1) is used with $\alpha = 1$ and a reduced energy

$$a = \frac{E_i^{\text{ion}} - E_i}{k_B T_e}$$

where E_i^{ion} is the energy of the ground state of the ion related to that of the ground state of the atom.

2. *Molecular Elementary Processes*

The kinetic mechanism comprises 1) dissociation of N_2, O_2, and NO by atomic or molecular impact/recombination; 2) dissociation of N_2 by electron impact/recombination; 3) associative ionization/dissociative recombination; 4) radical reactions (including Zel'dovich reactions); and 5) charge exchange.

For direct dissociation by molecular impact, the rate coefficients of Park et al. [30] are computed at the average temperature $(TT_{vi})^{1/2}$, where i stands for the index of the molecule being dissociated. Many models for the vibration-dissociation coupling have been developed in the last years [34–36]. Candler and Nompelis [37] mention that it is sometimes difficult to interpret the experimental data used to derive the constants for the Arrhenius expression for the forward reaction rate, a critical issue associated with the choice of these models. In many cases, the reaction rates were measured in shock-heated gas when the gas may be in thermochemical nonequilibrium. It is important to interpret the experimental data in a manner that is consistent with the vibration-dissociation model being used. Park [38,39] has made an extensive study of air reaction rates in the light of the $T - T_v$ model.

The reverse rates are computed at the gas temperature T based on the equilibrium constant. The rates of the nitrogen dissociation reaction by electron impact and of the reverse process are computed at the electron temperature T_e based on the same reference.

Zel'dovich reactions are known to greatly influence the distribution of nitrogen and oxygen between atomic and molecular systems and contribute to the destruction of O_2 and N_2 and the formation of NO. We have used the rate coefficients obtained by Bose and Candler [40,41] using a quasi-classical trajectory method performed starting from an ab initio potential surfaces calculation.

The dissociative recombination of the molecular ions is known to play a important role in the case of recombining plasmas [42,43]. In addition, the inverse process (associative ionization) allows for formation of the first electrons in many cases, such as in shock tubes and reentry problems and consequently explains many ionizing situations. In our case, because N_2^+, O_2^+, and NO^+ are present in the plasma described here, dissociative recombination has to be considered.

We have extracted the rate coefficients compiled by Teulet et al. [16], Capitelli et al. [44], and Kossyi et al. [45] related to charge transfer (with possible reassociation of atoms to form a molecule), reassociation, excitation transfer, ionization, and dissociation. Because of the pressure levels involved in our CR model, we have also taken into account the previous processes occurring when a third particle interacts. For further details, refer to [14].

3. *Radiative Processes*

At speeds higher than 10 km/s, the radiative signature of heated N_2 and O_2 mixtures is mainly due to the spontaneous emission of the N and O atoms. Because our atomic model is based on grouping elementary levels with similar characteristics, the equivalent spontaneous emission probability of each level has to be determined. Related data taken from the National Institute of Standards and Technology database [46] are given in Table 2. In total, we take into account 45 spontaneous emission lines for N and 24 lines for O. The possible reabsorption of radiation is estimated, making use of an escape factor α. In the following analysis, we assume that an optically thin medium is described by a value of $\alpha = 1$, whereas for an optically thick medium, $\alpha = 0$.

Table 2 Probability $A_{i\to j}$ for N(i) → N($j < i$) + $h\nu$ and O(i) → O($j < i$) + $h\nu$ spontaneous emission

i for N(i)	j for N(j)	$A_{i\to j}(s^{-1})$	i for O(i)	j for O(j)	$A_{i\to j}(s^{-1})$
6	1	2.30×10^8	5	1	3.80×10^8
4	1	5.40×10^8	9	1	1.77×10^8
5	2	5.50×10^8	11	1	0.38×10^8
5	3	2.00×10^8	14	1	2.30×10^8
13	2	4.60×10^8	19	1	6.77×10^7
13	3	0.52×10^8	17	2	4.50×10^8
10	6	4.05×10^6	6	4	0.34×10^8
17	2	8.60×10^3	12	4	3.26×10^5
18	2	0.65×10^8	7	5	0.28×10^8
20	2	0.47×10^8	13	5	6.60×10^5
16	3	1.30×10^8	8	6	2.72×10^7
18	3	5.80×10^3	10	6	4.19×10^7
20	3	1.30×10^8	15	6	0.71×10^7
15	2	1.10×10^8	18	6	7.01×10^6
15	3	0.20×10^8	23	6	3.05×10^6
22	6	0.25×10^6	25	6	1.23×10^6
23	6	0.37×10^6	9	7	1.88×10^7
25	6	0.43×10^6	11	7	2.35×10^7
28	2	0.33×10^8	14	7	2.90×10^7
8	4	0.19×10^8	16	7	0.62×10^7
9	4	2.28×10^7	19	7	3.25×10^6
10	4	3.18×10^7	24	7	2.34×10^6
11	5	2.17×10^7	12	8	4.50×10^6
12	5	2.86×10^7	12	10	4.70×10^5
31	5	1.70×10^6	——	——	——
31	13	1.59×10^7	——	——	——
22	4	0.02×10^8	——	——	——
23	4	0.73×10^7	——	——	——
25	4	0.25×10^7	——	——	——
21	5	2.34×10^6	——	——	——
16	7	2.56×10^7	——	——	——
17	8	3.73×10^7	——	——	——
19	8	9.92×10^6	——	——	——
17	9	7.46×10^4	——	——	——
18	9	6.30×10^6	——	——	——
19	9	2.48×10^7	——	——	——
18	10	5.72×10^6	——	——	——
18	11	1.16×10^7	——	——	——
20	11	0.06×10^8	——	——	——
14	8	1.47×10^7	——	——	——
14	9	0.76×10^7	——	——	——
27	8	3.89×10^6	——	——	——
27	9	2.12×10^6	——	——	——
38	7	2.30×10^5	——	——	——
37	9	6.10×10^5	——	——	——

C. Shock-Tube Flow Solver

We have developed a one-dimensional flow solver, SHOCKING, to simulate air plasmas obtained in shock-tube facilities, based on the model presented in [23]. This model has been modified to simulate reentries at speeds higher than 10 km/s. First, a radiative source term Q_{rad} has been added in the equation that expresses conservation of the total energy. Indeed, radiative transitions tend to deplete the flow energy for an optical thin medium. Second, a separate equation for the energy of the free electrons has been considered because the flow is significantly ionized.

1. *Conservation Equations*

Postshock conditions are derived from jump relations, assuming frozen-gas composition and vibrational and electronic energy modes, and the rotational mode is in equilibrium with the translational mode. Then the downstream flowfield is found by solving conservation equations of mass, momentum, global energy, and vibrational energy of the N_2, O_2, and NO molecules. A separate energy equation for the free electrons and species with electronic energy level populations is assumed to follow Boltzmann distributions:

$$\frac{\partial}{\partial x}(\rho_i u) = M_i \dot{\omega}_i, \qquad i \in \mathcal{S} \tag{2}$$

$$\frac{\partial}{\partial x}(\rho u^2 + p) = 0 \tag{3}$$

$$\frac{\partial}{\partial x}\left[\rho u\left(h + \frac{1}{2}u^2\right)\right] = -Q^{\text{rad}} \tag{4}$$

$$\frac{\partial}{\partial x}(\rho u y_m e_m^V) = M_m \dot{\omega}_m e_m^V + \Omega_m^{VT} + \Omega_m^{VV} - \Omega_m^{EV}, \qquad m \in \mathcal{V} \tag{5}$$

$$\frac{\partial}{\partial x}\left[\rho u\left(y_e e_e + \sum_{i\in\mathcal{E}} y_i e_i^E\right)\right] = -p_e \frac{\partial u}{\partial x} + M_e \dot{\omega}_e e_e + \sum_{i\in\mathcal{E}} M_i \dot{\omega}_i e_i^E - \Omega^I - \Omega^E + \Omega^{ET} + \Omega^{EV} \tag{6}$$

where $\mathcal{S}$ stands for the set of indices of the mixture species; $\mathcal{V}$ is the set of indices of the N_2, O_2, and NO molecules; $\mathcal{E}$ is the set of indices of the N^+, O^+, N_2, O_2, NO, N_2^+, O_2^+, and NO^+ species, for which the electronic energy populations are assumed to follow Boltzmann distributions; and $\mathcal{N}$ and $\mathcal{O}$ stand for the set of indices of the electronic energy levels of the N and O atoms. Thus, the set of indices of the heavy particles is given by $\mathcal{H} = \mathcal{N} \cup \mathcal{O} \cup \mathcal{E}$ and the set of the mixture species is given by $\mathcal{S} = \mathcal{H} \cup \{e\}$. The mass density of species i reads ρ_i and its molar mass M_i. The mixture mass density is given by the expression

$$\rho = \sum_{j\in\mathcal{S}} \rho_j$$

The mixture energy

$$e = \sum_{j\in\mathcal{S}} y_j e_j$$

The mass fraction $y_i = \rho_i/\rho$, mixture enthalpy $h = e + p/\rho$, and pressure

$$p = \rho RT \sum_{j\in\mathcal{H}} \frac{y_j}{M_j} + \rho RT_e \frac{y_e}{M_e}$$

The species energy e_i ($i \in \mathcal{S}$) comprises the translational and formation contributions $[e_e = e_e^T(T_e) + e_e^F]$ for electrons; the translational, electronic, and formation contributions $[e_i = e_i^T(T) + e_i^E + e_i^F]$ for the electronic energy states N(i) ($i \in \mathcal{N}$) and O(i) ($i \in \mathcal{O}$); the translational, electronic, and formation contributions

$$[e_i = e_i^T(T) + e_i^E(T_e) + e_i^F]$$

for the N^+ and O^+ ions; and the translational, rotational, vibrational, electronic, and formation contributions

$$[e_i = e_i^T(T) + e_i^R(T) + e_i^V(T_{\rm vi}) + e_i^E(T_e) + e_i^F]$$

for all of the molecules, where $T_{\rm vi}$ is the vibrational temperature of the i molecule. The number of electronic levels used to compute the energy of the ions and molecules is tuned to yield the best matching agreement between values of the computed energies and the reference tables of Gurvich et al. [47]. Energy of molecules is computed assuming the rigid rotor and harmonic oscillator approximations. Spectroscopic constants are taken from [47]. Electronic-specific data have been used for the vibrational and rotational constants of the molecules. In general, such simplified thermodynamic models for the rotation and vibration of molecules are not good approximations in high-temperature flow conditions. However, our results are relatively insensitive to the model chosen in this work, because the fraction of bound molecules is very low.

2. Energy Relaxation Terms

Radiative losses are modeled by means of the $Q_{\rm rad}$ term in the energy equation. This term represents the radiant power emitted per unit volume and is directly given by the expressions

$$Q^{\rm rad} = \alpha \sum_{\substack{i,j\in\mathcal{N}\\ j<i}} (E_i - E_j) A_{ij} N_i + \alpha \sum_{\substack{i,j\in\mathcal{O}\\ j<i}} (E_i - E_j) A_{ij} N_i \qquad (7)$$

where A_{ij} is the Einstein coefficient, N_i is the number density of the excited state, and α is the escape factor.

At high speeds, it is important to account for the energy lost by the free electrons during ionization and excitation of the atoms and molecules, as already stressed in [48,49]. Otherwise, electron-impact ionization reactions and, in general, all the reactions involving free electrons produce a large amount of free electrons without depleting their kinetic energy, thus enhancing their production. This phenomenon may lead to an avalanche ionization with consequent related numerical problems, especially for high-speed conditions. Here is an expression for the related source terms for electron-impact ionization and excitation reactions:

$$\Omega^I = \sum_{r\in\mathcal{R}^I} \dot{\omega}_{e,r} \mathcal{U}^r, \qquad \Omega^E = \sum_{r\in\mathcal{R}^E} \dot{\omega}_{e,r} \mathcal{U}^r \qquad (8)$$

where $\mathcal{U}^r$ is the reaction enthalpy of the r reaction, $\dot{\omega}_{e,r}$ is the electron chemical production term of the r reaction, $\mathcal{R}^I$ denotes the set of indices of the electron-impact ionization reactions, $\mathcal{R}^E$ is the set of indices of electron-impact excitation reactions, Ω^I accounts for the energy removed by electron-impact ionization reactions, and Ω^E accounts for the energy removal by electron-impact excitation reactions.

The rate of vibrational-translational energy transfer follows a Landau–Teller formula:

$$\Omega_m^{\rm VT} = \rho_m \frac{e_m^V(T) - e_m^V(T_{vm})}{\tau_m^{\rm VT}(T)}, \qquad m \in \mathcal{V} \qquad (9)$$

The average relaxation time is given by quantity

$$\tau_m^{\rm VT} = \sum_{j\in\mathcal{H}} \frac{\rho_j}{M_j} \Big/ \sum_{j\in\mathcal{H}} \frac{\rho_j}{M_j \tau_{mj}^{\rm VT}}$$

where the species relaxation time $\tau_{mj}^{\rm VT}$ is based on the Millikan–White formula, including Park's [48] correction. For the vibrational–vibrational energy exchange, different formulations have been tested. The one proposed by Candler and MacCormack [3] and modified by Knab et al. [9] has been chosen:

$$\Omega_m^{\rm VV} = \sum_{l\in\mathcal{V}} \mathcal{N}_A \sigma_{ml} P_{ml} \sqrt{\frac{8RT}{\pi\mu_{ml}}} \frac{\rho_l}{M_l} \rho_m \left(e_m^V(T) \frac{e_l^V(T_{vl})}{e_l^V(T)} - e_m^V(T_{vm}) \right) \qquad (10)$$

where the exchange probability P_{ml} is assumed to be equal to 10^{-2}, as suggested in [3], μ_{ml} denotes the reduced molar mass, and $\mathcal{N}_A$ is Avogadro's number.

The energy lost by electrons through elastic collisions with heavy particles is written as follows:

$$\Omega^{ET} = \frac{\frac{3}{2} n_e k_B (T - T_e)}{\tau_e^{ET}(T_e)} \qquad (11)$$

The relaxation time is obtained from kinetic theory:

$$\frac{1}{\tau_e^{ET}} = \sum_{j\neq e} \frac{m_e}{m_j} \nu_{ej}$$

where the collision frequencies read $\nu_{ej} = (8/3) v_e n_j \bar{\Omega}_{ej}^{11}$.

To model the exchange between the vibrational energy and the free-electron energy, we only consider molecular nitrogen, because this molecule is more efficient than O_2 and NO for this kind of process. This rate is assumed to follow a Landau–Teller formula:

$$\Omega^{EV} = \rho_{N_2} \frac{e_{N_2}^V(T_{v_{N_2}}) - e_{N_2}^V(T_e)}{\tau_e^{EV}(T_e)}. \qquad (12)$$

The relaxation time taken from [50] is preferred to the analytical form of Lee [51] that overestimates the relaxation time by a factor of 2.3 [50].

Following the derivation of Thivet [52], the conservative system of Eqs. (2–6) is transformed into a system of ordinary differential equations easily solved by means of the LSODE [53] library.

III. Results

In this section, we apply the collisional-radiative model previously described to Fire II, a well-known flight experiment from the 1960s. One of the primary objectives of the Fire project was to define the radiative heating environment associated with the reentry of a large-scale Apollo vehicle at a velocity of 11.4 km/s. During this reentry, a large portion of the overall wall heat flux was due to radiation. Most of the radiation (approximately 90%) came from atomic lines [13], and thus an accurate prediction of the populations of excited electronic states of the atoms is crucial. The aim of the present work is to test the CR model for different physicochemical conditions, from electronic energy level populations in strong nonequilibrium to populations following Boltzmann distributions. Starting from the earliest trajectory points, we move to a description of a point approaching peak heating.

The first part of this section is devoted to thermal nonequilibrium effects in the flow. We study the influence of separating the free-electron energy from the vibrational energy and compare our results for temperature and ionization degree with literature data. The rest of the section is devoted to a detailed analysis of the physicochemical state of the plasma for three trajectory points: 1634, 1636, and 1643 s

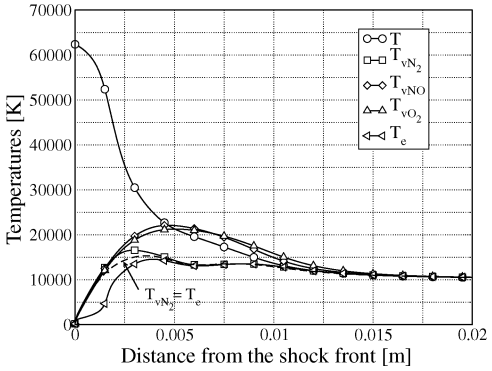

a) Temperature profiles

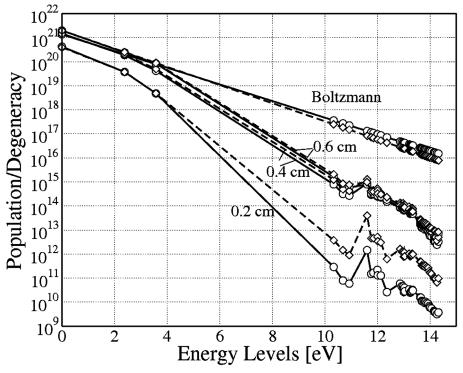

b) Electronic energy level populations for atomic nitrogen [m^{-3}]: CR model at 0.2, 0.4, and 0.6 cm; Boltzmann distribution at 0.4 cm

Fig. 1 Plots for the 1634 s case showing a comparison between the five-temperature model with $T_{vN_2} \neq T_e$ (solid line) and the four-temperature model with $T_{vN_2} = T_e$ (dashed line).

elapsed time from the launch. The validity of the QSS assumption that is often used to compute the excited electronic states is investigated for the 1634 s case by comparing the electronic energy level populations of atomic nitrogen obtained with the QSS assumption with the populations obtained by means of the full CR model.

The set of shock-tube operating conditions corresponding to the three trajectory points investigated here can be found in Table 3. Freestream characteristic quantities are denoted by the subscript 1, postshock characteristic quantities are denoted by the subscript 2, and u stands for the shock velocity. The mole fractions of nitrogen and oxygen are assumed to be constant through the shock ($x_{N_2} = 0.79$ and $x_{O_2} = 0.21$). We recall that after the shock, the rotational temperature is equal to the postshock gas temperature T_2, whereas the vibrational and electron temperatures are still equal to the freestream gas temperature T_1.

A. Analysis of the Fire II 1634 s Case

We investigate the physicochemical state of the plasma corresponding to the 1634 s trajectory point. We show that the flow is characterized by strong thermochemical nonequilibrium and depleted populations of the upper electronic energy levels of atoms.

1. *Thermal Relaxation*

In this section, we estimate the influence of the assumption of thermal equilibrium between the free-electron energy/Boltzmann electronic energy and the vibrational energy of N_2 on the results. Two different assumptions are used:

1) Two separate temperatures are used: T_{vN_2} for the vibration of N_2 and T_e for the translation of the free electrons and electronic excitation of the species following a Boltzmann distribution.

2) One common temperature $T_{vN_2} = T_e$ is used for all these energy modes. After the shock, no electrons are present because we have assumed the chemistry to be frozen in the jump relations.

Moreover, the electronic populations of molecular nitrogen and oxygen follow Boltzmann distribution at the freestream temperature T_1. Figure 1 shows how thermal nonequilibrium ($T_{V_{N_2}} \neq T_e$) is restricted to a narrow zone after the shock (≤ 0.4 cm) and has a negligible influence on the evolution of the postshock temperatures and electronic energy populations for atomic nitrogen. The populations of the higher energy levels computed based on $T_{vN_2} = T_e$ are overestimated in this zone. The thermal nonequilibrium zone is associated with a small electron number density (see Fig. 2). As soon as the electron density becomes significant, thermal relaxation is very fast, via the efficient EV energy-exchange processes.**

**Note that thermal nonequilibrium could have been even larger if the relaxation time of Lee [51] had been used instead of that of Bourdon and Vervisch [50].

Judging these discrepancies negligible, we have decided to assume that $T_{vN_2} = T_e$ in the remainder of this work and to solve the following equations:

$$\frac{\partial}{\partial x}\left[\rho u\left(y_{N_2} e^V_{N_2} + y_e e_e + \sum_{i\in\mathcal{E}} y_i e^E_i\right)\right] = M_{N_2}\dot{\omega}_{N_2} e^V_{N_2} + \Omega^{VT}_{N_2} + \Omega^{VV}_{N_2} - p_e\frac{\partial u}{\partial x} + M_e\dot{\omega}_e e_e + \sum_{i\in\mathcal{E}} M_i\dot{\omega}_i e^E_i - \Omega^I - \Omega^E + \Omega^{ET} \tag{13}$$

$$\frac{\partial}{\partial x}(\rho u y_m e^V_m) = M_m\dot{\omega}_m e^V_m + \Omega^{VT}_m + \Omega^{VV}_m, \qquad m \in \{O_2, NO\} \tag{14}$$

instead of Eqs. (5) and (6).

In Fig. 2a, we compare our four-temperature profiles ($T = T_r$, $T_{vN_2} = T_e$, T_{vO_2}, and T_{vNO}) with the two-temperature profiles ($T = T_r$ and $T_v = T_e$) obtained by Johnston [13]. Although the vibrational free-electron temperature results agree quite well, discrepancies are found in the relaxation of the rotranslational temperature. As explained by the method for capturing the shock, we have solved the Rankine–Hugoniot relations, as opposed to the shock-slip condition used by Johnston. Figure 2b shows the electron number density for different values of the escape factor α (from 0 to 1) and allows for the influence of the optical thickness on the results to be emphasized. We can appreciate how the free-electron number density rises rapidly after a distance of 0.4 cm due to the electron-impact ionization reactions. In the optically thick case ($\alpha = 0$), the electron population reaches an asymptotic value, whereas in the optically thin case ($\alpha = 1$), the curve exhibits a maximum after which the plasma loses energy and recombines due to radiative cooling.

In the same figure, we have also plotted the electron number density obtained by means of the two-temperature model of Park et al. [30], assuming a Boltzmann distribution among the electronic energy levels. The rate of ionization obtained in this case is higher.

2. *Composition and Electronic Energy Populations*

Characterization of the physicochemical state of the plasma in the shock layer requires the knowledge of the chemical composition as well as the determination of the energy stored into the internal modes. In Fig. 3, we examine the evolution of the different species concentrations. We recall that only molecular nitrogen and oxygen are present after the shock. These molecules first dissociate (in particular, molecular oxygen tends to completely disappear in favor of atomic oxygen right after the shock), whereas the full dissociation of molecular nitrogen is delayed. Ionization occurs simultaneously and produces free electrons, because nitrogen atom ionization is more efficient than ionization of the other species. Figure 3b shows

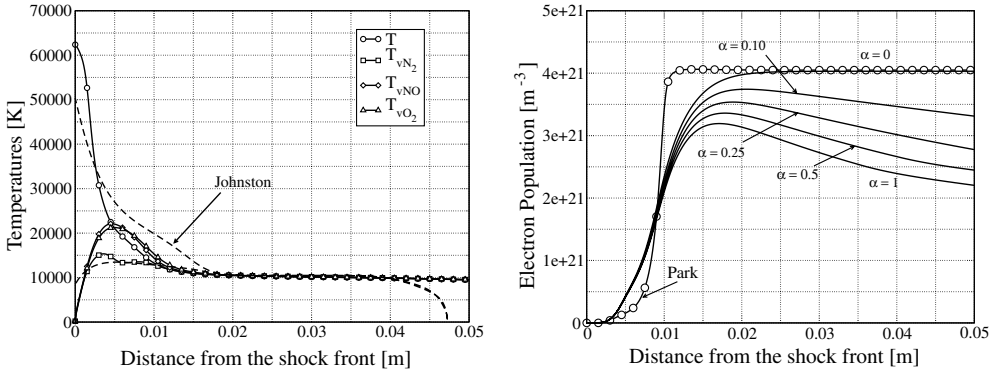

a) b)

Fig. 2 Plots for the 1634 s case showing a) temperature profiles for the CR model (solid line) and Johnston's [13] results (dashed line) and b) electron number density profiles for the CR model with escape factor values of 0, 0.1, 0.25, 0.5, and 1 (solid line) and the simplified kinetic mechanism of Park et al. [30] (line with circles).

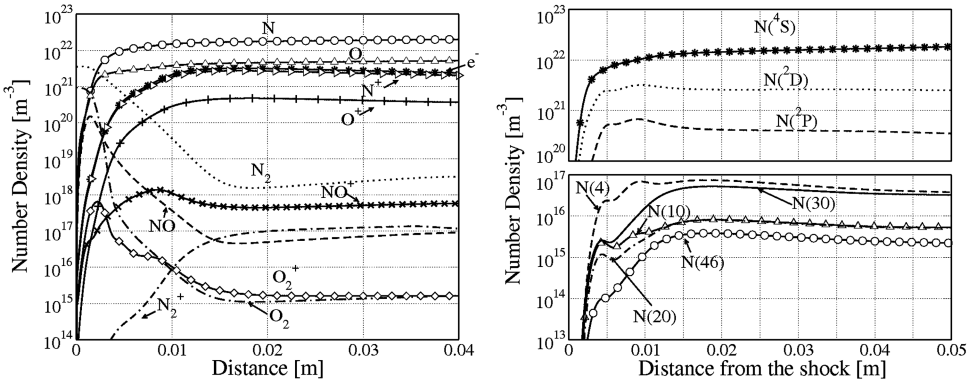

a) b)

Fig. 3 Plots for the 1634 s case showing number density profiles for a) mixture species and b) electronic states of atomic nitrogen.

electronic-state-specific population profiles for atomic nitrogen. Note that the upper electronic states are more reactive than the ground state and lower (metastable) states. Immediately after the shock, the populations of the excited levels tend to equilibrate with the free-electron populations that are in nonequilibrium. Moreover, we can observe how the atom populations are mainly in the ground electronic state at the beginning of the relaxation, consistent with the kinetic mechanism, assuming that dissociation of molecular nitrogen and oxygen generates atoms in the ground state:

$$\mathrm{N}_2 + M \rightleftharpoons \mathrm{N}(1) + \mathrm{N}(1) + \mathrm{M}$$

$$\mathrm{O}_2 + \mathrm{M} \rightleftharpoons \mathrm{O}(1) + \mathrm{O}(1) + \mathrm{M}$$

The same assumption holds for all of the other reactions (in particular, for the Zel'dowich reaction responsible for the atomic nitrogen formation). This assumption is justified because electronic excitation mainly occurs via electron impacts; the number density of electrons is still low in the postshock region.

After this incubation distance, the number density of electrons significantly increases and the electronic states of atoms thermalize. The electron-impact excitation processes

$$\mathrm{O}(i) + \mathrm{e}^- \rightleftharpoons \mathrm{O}(j) + \mathrm{e}^-, \qquad \mathrm{N}(i) + \mathrm{e}^- \rightleftharpoons \mathrm{N}(j) + \mathrm{e}^-$$

are fast and the populations of excited electronic states rapidly increase. The upper states are then depleted (in particular, by ionization and spontaneous emission), which explains the maximum found in the population profiles.

To characterize nonequilibrium of the populations, the number density of the electronic states of atomic nitrogen is compared in Fig. 4 with the Boltzmann and Saha distributions at two locations after the shock. Both Boltzmann and Saha distributions are computed based on the electron temperature T_e by keeping the atomic nitrogen concentration constant. In logarithmic scale, they appear as two parallel straight lines of slope proportional to $-1/T_e$.

In Fig. 4a, at 0.7 cm from the shock, the CR model predicts that the ground and metastable states follow the Boltzmann distribution, whereas the number density of the highly excited states is much lower and tends to the Saha distribution. This phenomenon is typical of nonequilibrium conditions encountered during high-speed reentries. Excellent agreement is found with the results presented in [13].

Figure 4b shows the same quantities at 2.5 cm from the shock. Because we have moved a further distance from the shock front, the flow tends toward equilibrium, and the Saha distribution tends to the Boltzmann distribution. Our model predicts that the high-lying excited states are still being depleted by radiative exchange with lower states. We notice that the comparison with literature is not as good at this location. Our results show a higher degree of nonequilibrium than in [13], closer to the Boltzmann distribution.

3. Standard QSS Approach

Quasi-steady-state models are often used in the literature [2,13] to study electronic energy level populations in strong nonequilibrium conditions, under which the hypothesis of a Boltzmann distribution does not hold. They constitute a valid alternative to the time-dependent CR model presented in this paper when the characteristic time of the excited state processes is very short with respect to the characteristic time of the flow. As a consequence, the set of mass conservation equations for the electronically excited states given in Eq. (2) can be expressed as a set of nonlinear algebraic equations to be solved separately from the other conservation equations. It is important to emphasize that this operation does not reduce the computational cost if the electronic energy populations are computed everywhere in the flow. The QSS assumption is only desirable when the populations of excited states are probed at some locations of

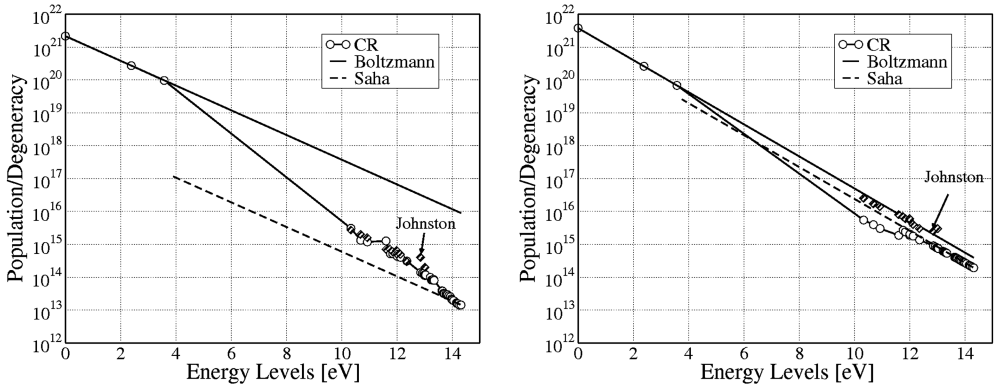

a) 0.7 cm from the shock front b) 2.5 cm from the shock front

Fig. 4 Plots for the 1634 s case showing electronic energy level populations for atomic nitrogen (m^{-3}). Johnston's [13] results are shown in black diamonds.

interest (for instance, along the stagnation line in multidimensional flow simulations), therefore allowing for a drastic reduction of the computational cost versus the time-dependent CR model.

It is well known that the regime of validity of the QSS assumption is strongly influenced by a sudden change in the plasma conditions, such as after a strong shock, when the electron density is very scarce. Because the collisional processes are responsible for the equilibration of the internal energy states (in particular, the processes involving electrons as collision partners), a lack of electrons contributes to the failure of the QSS assumption.

In this section, we compare the results obtained by means of the time-dependent CR model with the standard QSS methods presented in [2,13]. First, we compute the profiles of the flow characteristic quantities (pressure, temperatures, and composition) based on the effective reaction rates of Park et al. [30] for air chemistry that are widely used in the literature but different from the mechanism given in Sec. II. Then the QSS populations of excited states are computed at a given location by solving the following system of ordinary differential equations:

$$\frac{d}{dt}y_i = \frac{M_i\dot{\omega}_i}{\rho}, \qquad i \in \mathcal{N}_1 \cup \mathcal{O}_1 \tag{15}$$

where the index i runs over all the excited states of N and O, including the metastable states. In our approach, formally different from the system of nonlinear algebraic equations described by the law of mass action, $\dot{\omega}_i = 0\,(i \in \mathcal{N}_1 \cup \mathcal{O}_1)$ has an equivalent solution for $t \to \infty$. Our method presents the advantage of overcoming numerical problems that are sometimes encountered when using the algebraic formulation [2,13]. The population of the ground states is retrieved by ensuring that the total number density computed during the flow calculation is conserved in the QSS calculation.

In the following analysis, we examine the first trajectory point at a location of 0.7 cm from the shock front. We compute the electronic energy populations of nitrogen atoms based on three models:

1) Full CR is the time-dependent CR model described in Sec. II.

2) QSS Abba is the QSS model with the same data for the atomic and radiative elementary processes as in the full CR model.

3) QSS Park is the QSS model with the energy levels and data for the atomic and radiative elementary processes of Park [2].

The main differences between the various models are the coupling method and the sets of data for the reaction rates. For both QSS models, the flow calculations have been performed by clipping the reaction rates of [30] to avoid using them out of their validity range; the translational temperature driving the rate constants has been limited to the value of 30,000 K. Moreover, the free-electron energy loss term for electron-impact ionization given in Eq. (13) is computed based the expression suggested in [13]:

$$\Omega^I = -\omega_{N^+} I^{N^+} - \omega_{O^+} I^{O^+} \tag{16}$$

where

$$I^{N^+} = 4.05 \times 10^8 \text{ J/(kg} \cdot \text{mol)},$$
$$I^{O^+} = 4.30 \times 10^8 \text{ J/(kg} \cdot \text{mol)}$$

In the full CR model, we recall that this term is directly computed based on Eq. (8) from the expressions for the reaction rates intrinsic to the model, without any a priori hypothesis. Figure 5 shows a comparison between the results obtained by means of the three models, the Boltzmann distribution, and Johnston's [13] results. The full CR model and the QSS Abba model yield electronic energy level populations in rather good agreement with Johnston's results. The QSS Abba model slightly underpredicts the population of the lower electronic levels. The QSS assumption is a fair approximation at this location. The differences between the QSS Abba results and the QSS results of Johnston are not well understood. They might be explained by the different data for the electron-impact excitation rates of atoms or for the radiative processes. The differences with respect to the QSS Park model for atomic and radiative processes are significant: up 2 orders of magnitude for the upper levels above the metastable states. A comparison with accurate quantum mechanical calculation [54,55] shows that Park's model tends to overestimate the rate constants for some bound transition [13,56]. As a consequence, Park's model yields results that are closer to equilibrium.

In conclusion, the standard QSS approach seems to be valid *at this location*, provided that a correct set of reaction rates is chosen for the model. This choice should be based on a comparison of the computed results with experimental data.

In the flow calculation, the need for a special adjustment for the effective rate constants of Park et al. [30] (maximum temperature) and for the source term responsible for the energy removal from the free-electron temperature makes it difficult to extrapolate to generic flow conditions.

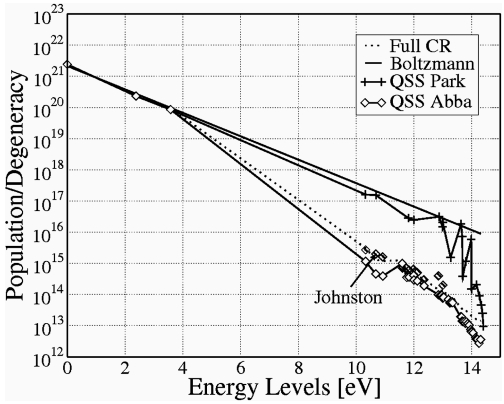

Fig. 5 Plots for the 1634 s case, 0.7 cm from the shock front, showing electronic energy level populations for atomic nitrogen (m^{-3}). Johnston's [13] results are shown with black diamonds.

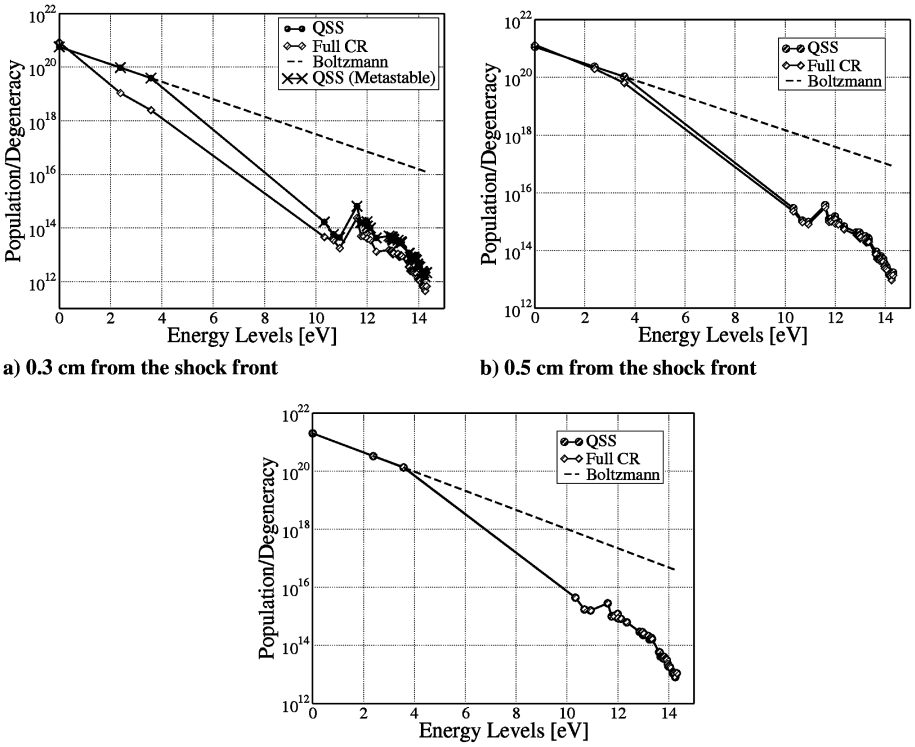

a) 0.3 cm from the shock front

b) 0.5 cm from the shock front

c) 1 cm from the shock front

Fig. 6 Plots for the 1634 s case showing electronic energy level populations for atomic nitrogen (m^{-3}).

4. Toward a Simplified CR Model

In the foregoing section, we have studied the standard QSS approach by comparing QSS results and time-dependent CR results at one location in the flow. In this comparison, the reaction rate data are not identical: for instance, the rates of molecular elementary processes used in the full CR model differ from the rates used in the QSS Abba model. In this section, we further investigate the validity of the QSS assumption based on the same set of reaction rates at several locations in the flow. This is a preliminary step to derive a simplified CR model for reentries at speeds higher than 10 km/s, which are typical of moon returns.

For this purpose, we compute the electronic energy populations of atomic nitrogen for the first trajectory point (1634 s case) by means of the full CR model. From the calculation, we extract the profiles of the flow characteristic quantities (pressure, temperatures, and composition). Then the QSS populations of excited electronic states are computed at a given location by solving the system of Eqs. (15). This approach is called the *simplified CR model* in the following.

The QSS distribution of excited states is computed by solving the set of Eqs. (15). In the first model (simplified CR metastable), the index runs from $i = 2$ to the total number of electronic levels for the atomic species, whereas in the second model (simplified CR), the metastable states are considered in Boltzmann equilibrium with the ground state, and i starts from 4. The latter hypothesis is justified by the small difference in terms of electronic energy among the ground state and the two metastable states, which enhances the excitation due to impacts with light and heavy particles promoting thermalization. At the instant $t = 0$, the initial population is assumed to be Boltzmann at the prescribed pressure and temperature conditions.[††] A careful analysis of system (15) reveals that the population of the ground state and that of the two metastable states (for the second model, the simplified CR model) is needed to close the system of equations. In the first case, the population of the ground state is retrieved by summing the population of the excited states and subtracting this value to the total number density given by the flowfield calculation.

[††]The initial distribution does not have any influence on the results that depend only on temperature, pressure, and the total number of atoms.

The flow is investigated at three locations: 0.3, 0.5, and 1 cm from the shock. The electronic energy level populations for atomic nitrogen are shown in Fig. 6. At 0.3 cm, the populations obtained by means of the simplified CR model are higher than the populations obtained by means of the full CR model; the QSS assumption is not valid in the near-shock region. This difference of populations is much more pronounced for the metastable states that follow a Boltzmann distribution when the QSS assumption is used. At 0.5 cm, all the excited states practically satisfy the QSS condition. After 1 cm, no difference is noticed between the results obtained by means of the two models. An explanation is found by examining the characteristic time for the atomic excitation and ionization processes. For instance, we find that this characteristic time for the first metastable state is of the same order of magnitude as the characteristic time of the flow 5×10^{-6} s computed at 1 cm from the shock.

Based on this analysis, we recommend to keep the atomic metastable states as separate species for this trajectory point and compute the upper electronic states by means of a QSS model, to reduce the computational cost in multidimensional flow simulations. The CR model could be used as a tool to derive effective reaction rates for the simplified mechanism associated with this mixture of species and the expressions for the free-electron energy loss term for electron-impact ionization and ionization reactions.

B. Analysis of the Fire II 1636 s Case

1. Thermal Nonequilibrium Effects

To demonstrate that the one-dimensional flow solver SHOCKING is capable of reproducing the main physicochemical features along the stagnation line of reentry flows, except for the boundary-layer region, we compare our results with simulations obtained by means of the validated flow solvers LAURA and DPLR [31] and the viscous shock layer code of Johnston [13]. The comparison is carried out for the temperature and ionization profiles.

In Fig. 7a, we show profiles of the translational temperature and the molecular nitrogen vibrational temperature obtained by means of our CR model (T and $T_{v\mathrm{N}_2}$) and of the two-temperature reference models (T and T_v). Noticeable differences are found in the thermal relaxation zone. The postshock translational temperature obtained by means of the SHOCKING code from the Rankine–Hugoniot relations is much

higher than the values obtained by means of the LAURA and DPLR codes and closer to the value obtained by Johnston [13], who used a discrete boundary condition (shock-slip condition). Another possible source of discrepancies is the absence of dissipative effects in the CR model. The vibrational temperature obtained by means of the CFD codes is higher than the frozen value. Fair agreement can be observed among all the results for the vibrational temperature of N_2. This is very important, given its close association with radiation, electronic excitation, and electron density [21].

The optical thickness of the medium plays an important role in our simulations. The upper curve (labeled $\alpha = 0$) represents the optically thick case, and the lower curve (labeled $\alpha = 1$) represents the optically thin case. A lower temperature is obtained for an optically thin medium because the flow energy is depleted by radiation.

In Fig. 7b, we compare the results obtained for the ionization degree. In the case of an optically thick medium, it reaches a plateau; a fair agreement is found with the literature. Large differences are found when radiative cooling is taken into account because it reduces the degree of ionization. Our model predicts that the ionization process is more rapid than the model implemented into the LAURA code and into the viscous shock layer code.

2. *Electronic Energy Populations*

In Fig. 8, the electronic energy level populations are shown at 0.5 cm from the shock front for an electron temperature value of 12,883 K. We clearly see that the low electronic energy levels tend to follow a Boltzmann distribution at the electron temperature, whereas close to the ionization limit, the excited electronic states approach a Saha distribution at the electron temperature. Because the channels between the low- and high-lying electronic states exhibit finite ionization rates, a lack of free electrons may result in depleted populations for the highly excited states. The distribution is no longer of the Boltzmann type and the electronic temperature is no longer defined.

The departures from the Boltzmann distribution, which are of the same order of magnitude for atomic nitrogen and atomic oxygen, tend to reduce the radiative contribution to the overall heat flux in the earlier parts of the trajectory. For this reason, attempts to estimate the radiative flux assuming a Boltzmann distribution among electronic levels might lead to an overestimation of this heat flux.

C. Analysis of the Fire II 1643 s Case

In this section, we analyze a trajectory point close to peak heating. Figure 9a shows that the thermal nonequilibrium effects are located in a very narrow region near the shock. The electronic energy level populations of atomic nitrogen at 0.5 cm from the shock are given in Fig. 9b. Note that these populations follow Boltzmann distributions in the entire domain. These results are explained by the values of the postshock pressure p_2 given in Table 3, which are much higher than for the first two trajectory points. At high pressures, the plasma is dominated by collisional processes; thermal relaxation is enhanced and the electronic state populations tend toward Boltzmann distributions.

IV. Conclusions

In this work, we have studied the departure of the atomic electronic energy populations from Boltzmann distributions for one-dimensional airflows obtained in a shock-tube. The operating conditions are taken from three points in the trajectory of the Fire II flight experiment at 1634, 1636, and 1643 s elapsed time from the launch. The results have been obtained by means of a multitemperature fluid model fully coupled with an electronic-specific collisional-radiative model. We have compared the flowfield quantities and electronic energy populations with literature [13,31] and found a good agreement. We have also found that for the first two points of the trajectory (1634 and 1636 s), the electronic energy level

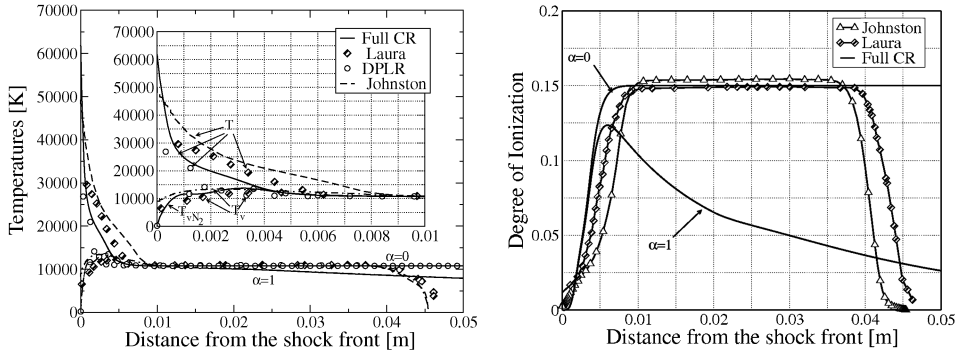

a) b)

Fig. 7 Plots for the 1636 s case showing a) temperature profiles compared with results from [13,31] (CR model had escape factor values of 0 and 1) and b) ionization degree profiles (LAURA results are denoted by the line with diamonds and Johnston's [13] results are denoted by the line with triangles).

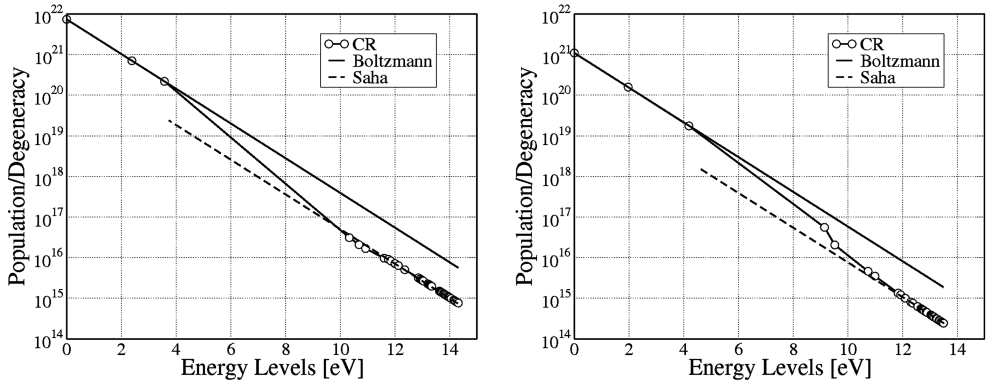

a) Atomic nitrogen **b) Atomic oxygen**

Fig. 8 Plots for the 1636 s case, 0.5 cm from the shock front, showing electronic energy level populations (m^{-3}).

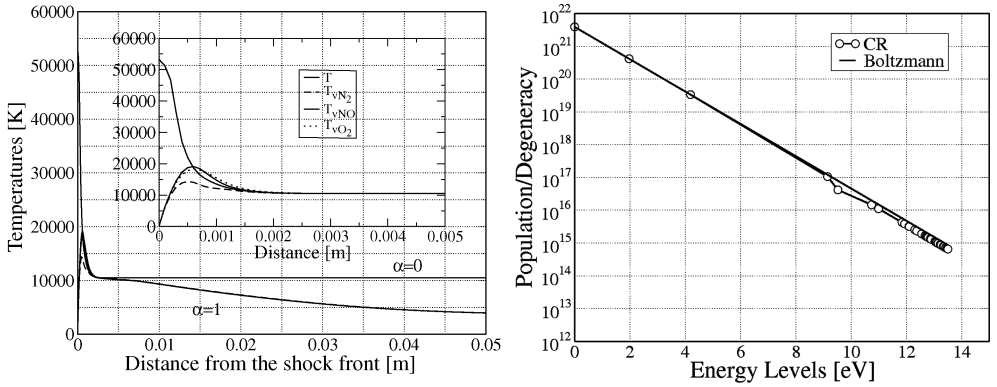

Fig. 9 Plots for the 1633 s case: a) temperature profiles with escape factor values of 0 and 1 and b) electronic energy level populations for atomic nitrogen (m^{-3}) 0.5 cm from the shock front.

populations of the N and O atoms depart from Boltzmann distributions because the high-lying bound electronic states are depleted. The analysis of the last trajectory point (1643 s) instead reveals a Boltzmann distribution among the electronic levels.

An analysis of the state of the flow for the first flight condition (1634 s) led us to the conclusion that the excited species of atoms satisfy the quasi-steady-state assumption, except for the two metastable states. As a consequence, the global rate coefficients and free-electron energy loss terms could be derived in the steady state based on our model, however, considering the metastable states as separate pseudospecies governed by their own chemical-kinetic mechanism.

Moreover, the validity of the standard QSS approach widely used by the aerospace community has been tested; the results obtained by means of our full CR model and the standard QSS model are found to be in good agreement. It is important to mention that the full CR model is more general, because the parameters governing the free-electron energy losses by electron-impact ionization are obtained from the expressions for the reaction rates intrinsic to the model, without any a priori hypothesis.

Finally, we have shown that the populations of high-lying excited states of atoms obtained by using the rates of Park [2] for electron-impact excitation and ionization reactions are up to 2 orders of magnitude higher than the populations obtained by using the rates of Bultel et al. [14], consistent with the result of Johnston [13].

We are currently adding the electronic energy levels of the molecules in the CR model [27] and plan to consider vibrational energy levels as well, accounting for vibrational nonequilibrium (non-Boltzmann distribution) of the molecules. These phenomena, generally less important in flows subjected to compression, might become relevant in expanding flow situations affecting the vibrational populations of molecular species that, as a consequence, can also depart from Boltzmann distributions. It is important to notice that a set of rovibrational rates is currently being computed at NASA Ames Research Center, based on first-principles calculations [57,58].

In a further work, we will use the detailed CR model described in the previous sections as a baseline to create new reduced kinetic mechanisms for airflow conditions that are typical of reentry applications. The number of electronic levels of atoms and molecules considered in the model will be reduced by grouping similar energy levels. This will allow us to extend the use of the CR model for 2-D and 3-D computational fluid dynamic simulations.

Table 3 Shock-tube flow characteristic quantities

	Time, s		
Flow quantities	1634	1636	1643
p_1, Pa	2.0	5.25	21.3
T_1, K	195	210	276
u_1, m/s	11,360	11,310	10,480
p_2, Pa	3827	9229	24,506
T_2, K	62,377	61,884	53,191
u_2, m/s	1899	1891	1756

Acknowledgments

The authors would like to acknowledge S. Macheret (Lockheed Martin Skunk Works) for suggestions on the free-electron energy model and C. O. Johnston (NASA Langley Research Center) for providing the results used in the comparison.

References

[1] Gnoffo, P. A., Gupta, R. N., and Shinn, J. L., "Conservation Equations and Physical Models for Hypersonic Air Flows in Thermal and Chemical Non-Equilibrium," NASA, TP 2867, 1989.

[2] Park, C., *Nonequilibrium Hypersonic Aerothermodynamics*, Wiley, Hoboken, NJ, 1989.

[3] Candler, G. V., and MacCormack, R. W., "Computation of Weakly Ionized Hypersonic Flows in Thermochemical Nonequilibrium," *Journal of Thermophysics and Heat Transfer*, Vol. 5, No. 3, 1991, pp. 266–273. doi:10.2514/3.260

[4] Laux, C. O., "Radiation and Nonequilibrium Collisional-Radiative Models," *Physicochemical Models for High Enthalpy and Plasma Flows*, 2002–2007 VKI Lecture Series, Vol. 1, von Kármán Inst. for Fluid Dynamics, Rhode-Saint-Genèse, Belgium, 4–7 July 2002, p. 55.

[5] Capitelli, M., Colonna, G., and Armenise, I., "State-to-State Electron and Vibrational Kinetics in One Dimensional Nozzle and Boundary Layer Flows," *Physicochemical Models for High Enthalpy and Plasma Flows*, 2002–2007 VKI Lecture Series, Vol. 1, von Kármán Inst. for Fluid Dynamics, Rhode-Saint-Genèse, Belgium, 4–7 July 2002, p. 21.

[6] Bourdon, A., and Bultel, A., "Detailed and Simplified Kinetic Schemes for High Enthalpy Air Flows and Their Influence on Catalycity Studies," *Experiment, Modeling and Simulation of Gas Surface Interaction for Reactive Flows*, 2005–2006 VKI Lecture Series, von Kármán Inst. for Fluid Dynamics, Rhode-Saint-Genèse, Belgium, 6–9 Feb. 2006, Vol. 1, 2006, p. 60.

[7] Sarma, G. S. R., "Physico-Chemical Modelling in Hypersonic Flow Simulation," *Progress in Aerospace Sciences*, Vol. 36, Nos. 3–4, Apr. 2000, pp. 281–349. doi:10.1016/S0376-0421(00)00004-X

[8] Bourdon, A., Leroux, P., and Vervisch, P., "Experiment-Modeling Comparison in a Nonequilibrium Supersonic Air Nozzle Flow," *Journal of Thermophysics and Heat Transfer*, Vol. 13, No. 1, 1999, pp. 68–75. doi:10.2514/2.6402

[9] Knab, O., Frühauf, H., and Messerschmid, E., "URANUS/CVCV Model Validation by Means of Thermochemical Nonequilibrium Nozzle Airflow Calculations," *Proceedings of the 2nd European Symposium on Aerothermodynamics for Space Vehicles*, ESA Publ. Div., Noordwijk, The Netherlands, 1994, p. 129.

[10] Surzhikov, S., Sharikov, I., Capitelli, M., and Colonna, G., "Kinetic Model of Nonequilibrium Radiation of Strong Air Shock Waves," AIAA Paper 2006-586, Jan. 2006.

[11] Surzhikov, S., Rouzaud, O., Soubrie, T., Gorelov, V., and Kireev, A., "Prediction of Non-Equilibrium and Equilibrium Radiation for Reentry Conditions," AIAA Paper 2006-1188, Jan. 2006.

[12] Park, C., "Thermochemical Relaxation in Shock Tunnels," *Journal of*

Thermophysics and Heat Transfer, Vol. 20, No. 4, 2006, p. 689. doi:10.2514/1.22719

[13] Johnston, C. O., "Nonequilibrium Shock-Layer Radiative Heating for Earth and Titan Entry," Ph.D. Thesis, Virginia Polytechnic Inst. and State Univ., Blacksburg, VA, 2006.

[14] Bultel, A., Cheron, B., Bourdon, A., Motapon, O., and Schneider, I., "Collisional-Radiative Model in Air for Earth Re-Entry Problems," *Physics of Plasmas*, Vol. 13, No. 4, 2006, p. 11.

[15] Sarrette, J.-P., Gomes A.-M., Bacri, J., Laux, C., and Kruger, C., "Collisional-Radiative Modeling of Quasi-Thermal Air Plasmas with Electronic Temperatures Between 2000 and 13000 K," *Journal of Quantitative Spectroscopy and Radiative Transfer*, Vol. 1, No. 2, 2001, pp. 53–125.

[16] Teulet, P., Sarrette, J.-P., and A.-M., G., "Collision-Radiative Modeling of One- and Two-Temperature Air and Air-Sodium Plasmas at Atmospheric Pressure with Temperatures of 2000–12000 K," *Journal of Quantitative Spectroscopy and Radiative Transfer*, Vol. 1, July 2001, pp. 70–159.

[17] Chauveau, S. M., Laux, C., Kelley, J. D., and Kruger, C., "Vibrationally-Specific Collisional-Radiative Model for Non-Equilibrium Air Plasmas," 33th AIAA Plasmadynamics and Lasers Conference, Maui, HI, AIAA Paper 2002-2229, 2002.

[18] Bose, D., Wright, M., Bogdano, D., Raiche, G., and Allen, G. A., "Modeling and Experimental Assessment of CN Radiation Behind a Strong Shock Wave," *Journal of Thermophysics and Heat Transfer*, Vol. 20, No. 2, 2006, p. 220. doi:10.2514/1.16869

[19] Park, C., "Nonequilibrium Air Radiation (NEQAIR) Program: User's Manual," NASA Ames Research Center, TM86707, Moffett Field, CA, 1985.

[20] Dunn, M. G., and Kang, S. W., "Theoretical and Experimental Studies of Reentry Plasmas," NASA CR-2232, 1973.

[21] Park, C., "Problems of Rates Chemistry in the Flight Regimes of Aeroassisted Orbital Transfer Vehicles," *Thermophysical Aspects of Re-Entry Flows*, edited by J. N. Moss, and C. D. Scott, AIAA, New York, 1986.

[22] Gupta, R. N., Yos, J. M., Thompson, R. A., and Lee, K. P., "A Review of Reaction Rates and Thermodynamic and Transport Properties for an 11-Species Air Model for Chemical and Thermal Non-Equilibrium Calculations to 30,000 K," NASA Reference Publ. 1232, Aug. 1990.

[23] Magin, T. E., Caillault, L., Bourdon, A., and Laux, C. O., "Nonequilibrium Radiative Heat Flux Modeling for the Huygens Entry Probe," *Journal of Geophysical Research*, Vol. 111, No. E7, 2006, pp. E07S12. doi:10.1029/2005JE002616

[24] Colonna, G., Capitelli, M., and Giordano, D., "State to State Electron and Vibrational Kinetics in Supersonic Nozzle Air Expansion: An Improved Model," AIAA Paper 2002-2163, May 2002.

[25] Cauchon, D. L., "Radiative Heating results from Fire II Flight Experiment at a Reentry velocity of 11.4 km/s," NASA Ames Research Center TM X-1402, Moffett Field, CA, 1967.

[26] Olynick, D., Henline, W. D., Hartung, L., and Candler, G., "Comparisons of Coupled Radiative Navier-Stokes Flow Solutions with the Project Fire II Flight Data," AIAA Paper 94-1955, June 1994.

[27] Panesi, M., Magin, T., Bourdon, A., Bultel, A., and Chazot, O., "Analysis of the Fire II Flight Experiment by Means of a Collisional-Radiative Model," 46th AIAA Aerospace Sciences Meeting and Exhibit, Reno, NV, AIAA Paper 2008-1205, Jan. 2008.

[28] Bose, D., McCorkle, E., and Thompson, C. e. a., "Analysis and Model Validation of Shock Layer Radiation in Air," AIAA Paper 2008-1246, Jan. 2008.

[29] Johnston, C., "A Comparison of the East Shock-Tube Data with a New Air Radiation Model," AIAA Paper 2008-1245, Jan. 2008.

[30] Park, C., Jae, R., and Partridge, H., "Chemical-Kinetic Parameters of Hyperbolic Earth Entry," *Journal of Thermophysics and Heat Transfer*, Vol. 15, No. 1, 2001, p. 76. doi:10.2514/2.6582

[31] Hash, D., Olejniczak, J., Wright, M., Prabhu, D., Pulsonetti, M., Hollis, B., Gnoo, P., Barnhardt, P., Nompelis, I., and Candler, G., "Fire II Calculations for Hypersonic Nonequilibrium Aerothermodynamics Code Verification: DPLR, LAURA, and US3-D," 45th AIAA Aerospace Sciences Meeting and Exhibit, Reno, NV, AIAA Paper 2007-605, Jan. 2007.

[32] Drawin, H., "Zur Formelmssigen Darstellung des Ionisierungsquerschnitts fur den Atom-Atomstoss und ber die Ionen-Elektronen-Rekombination im Dichten Neutralgas," *Zeitschrift fur Physik D: Atoms, Molecules and Clusters*, Vol. 211, No. 3, 1968, pp. 404–417.

[33] Drawin, H., "Atomic Cross Sections for Inelastic Electronic Collisions," Association Euratom-CEA, Rept. EUR-CEA-FC 236, Cadarache, France, 1963.

[34] Adamovich, I. V., MacHeret, S. O., Rich, J. W., and Treanor, C. E., "Vibrational Energy Transfer Rates Using a Forced Harmonic Oscillator Model," *Journal of Thermophysics and Heat Transfer*, Vol. 12, No. 1, 1998, pp. 57–65. doi:10.2514/2.6302

[35] Chernyi, G. G., and Losev, S. A., Macheret, S. O., and Potapkin, B. V., *Physical and Chemical Processes in Gas Dynamics: Physical and Chemical Kinetics and Thermodynamics of Gases and Plasmas*, AIAA, Reston, VA, 2004.

[36] Knab, O., Freuhauf, H., and Messerschmid, E., "Theory and Validation of the Physically Consistent Coupled Vibration-Chemistry-Vibration Model," *Journal of Thermophysics and Heat Transfer*, Vol. 9, No. 2, 1995, pp. 219–226. doi:10.2514/3.649

[37] Candler, G., and Nompelis, I., *Computational Fluid Dynamics for Atmospheric Entry*, VKI Lecture Series, Vol. 1, RTO-EN-AVT-162, von Kármán Inst. for Fluid Dynamics, Rhode-Saint-Genèse, Belgium, 2008.

[38] Park, C., "Assessment of a Two-Temperature Kinetic Model for Dissociating and Weakly Ionizing Nitrogen," AIAA Paper 86-1347, June 1986.

[39] Park, C., "Assessment of Two-Temperature Kinetic Model for Ionizing Air," AIAA Paper 87-1574, June 1987.

[40] Bose, D., and Candler, G., "Thermal Rate Constants of the N2 + O → NO + O Reaction Using Ab Initio 3 a and 3 a Potential-Energy Surfaces," *Journal of Chemical Physics*, Vol. 104, No. 8, 1996, p. 2825. doi:10.1063/1.471106

[41] Bose, D., and Candler, G., "Thermal Rate Constants of the O2 + N → NO + O Reaction Using Ab Initio 3 a and 3 a Potential-Energy Surfaces," *Journal of Chemical Physics*, Vol. 107, No. 16, 1997, p. 6136. doi:10.1063/1.475132

[42] Guberman, S. L. (ed.), *Dissociative Recombination of Molecular Ions with Electrons*, Kluwer Academic, New York, and Plenum, New York, 2003.

[43] Bultel, A., van Ootegem, B., Bourdon, A., and Vervisch, P., "Influence of Ar2 in an Argon Collisional Radiative Model," *Physical Review E (Statistical Physics, Plasmas, Fluids, and Related Interdisciplinary Topics)*, Vol. 65, No. 4, 2002, Paper 046406. doi:10.1103/PhysRevE.65.046406

[44] Capitelli, M., Ferreira, C., Gordiets, B., and Osipov, A., *Plasma Kinetics in Atmospheric Gases*, Springer, Berlin, 2000.

[45] Kossyi, I., Kostinsky, A., Matveyev, A., and Silakov, V., "Kinetic Scheme of the Non-Equilibrium Discharge in Nitrogen-Oxygen Mixtures," *Plasma Sources Science and Technology* , Vol 1, No. 3, 1992, p. 207. doi:10.1088/0963-0252/1/3/011

[46] Martin, W. C., Fuhr, J. R., Kelleher, D. R., Masgrove, A., Sugar, J., and Wiese, W. L., "NIST Atomic Spectra Database Version 3," http://physics.nist.gov/asd2, [retrieved 2008].

[47] Gurvich, L., Veyts, I., and Alcock, C., *Thermodynamic Properties of Individual Substances*, Vol. 1, Hemisphere, New York, 1989.

[48] Park, C., "Review of Chemical-Kinetic Problems of Future NASA Mission, 1: Earth Entries," *Journal of Thermophysics and Heat Transfer*, Vol. 7, No. 3, 1993, p. 385. doi:10.2514/3.431

[49] Roberts, T. P., "Implementation into TINA Modelling for Electron-Electronic Energy Equation," Thermophysics Conference, New Orleans, LA, AIAA Paper 1996-1851, June 1996.

[50] Bourdon, A., and Vervisch, P., "Electron-Vibration Exchange Models in Nitrogen Flows," *Physical Review E (Statistical Physics, Plasmas, Fluids, and Related Interdisciplinary Topics)*, Vol. 55, No. 4, 1997, p. 4634. doi:10.1103/PhysRevE.55.4634

[51] Lee, J. H., "Basic Governing Equations for the Flight Regimes of Aeroassisted Orbital Transfer Vehicles," AIAA Paper 84-1729, June 1984.

[52] Thivet, F., "Modeling and Computation of Hypersonic Flows in Chemical and Thermodynamic Non-Equilibrium," Ph.D. Thesis, Ecole Centrale Paris, Chatenay-Malabry, France, 1992 (in French).

[53] Radhakrishnan, K., and Hindmarsh, A., *Description and Use of LSODE: The Livermore Solver for Ordinary Differential Equations*, Vol. 1, NASA, 1993, p. 124.

[54] Tayal, S., "Effective Collision Strengths for Electron Impact Excitation of N," *Atomic Data and Nuclear Data Tables*, Vol. 76, No. 2, 2000, pp. 191–212. doi:10.1006/adnd.2000.0842

[55] Frost, R. M., Awakowicz, P., Summers, H. P., and Badnell, N. R.,

"Calculated Cross-Sections and Measured Rate Coefficients for Electron Impact Excitation of Neutral and Singly Ionized Nitrogen," *Journal of Applied Physics*, Vol. 84, No. 6, 1998, p. 2989. doi:10.1063/1.368452

[56] Huo, W. M., "Electron-Impact Excitation and Ionization in Air," AIAA Paper 2008-1207, Jan. 2008.

[57] Chaban, G., Jae, R., Schwenke, D., and Huo, W., "Dissociation Cross Sections and Rate Coefficients for Nitrogen from Accurate Theoretical Calculations," AIAA Paper 2008-1209, Jan. 2008.

[58] Jae, R., Schwenke, D., Chaban, G., and Huo, W., "Vibrational and Rotational Excitation and Relaxation of Nitrogen from Accurate Theoretical Calculations," AIAA Paper 2008-1208, Jan. 2008.